




# Neutron-skin values and matter and neutron radii determined from reaction cross sections of proton scattering on $^{12}\text{C}$ , $^{40,48}\text{Ca}$ , $^{58}\text{Ni}$ , and $^{208}\text{Pb}$

Tomotsugu Wakasa,<sup>1</sup> Shingo Tagami ,<sup>1</sup> Jun Matsui ,<sup>1</sup> Maya Takechi,<sup>2</sup> and Masanobu Yahiro <sup>1,\*</sup>

<sup>1</sup>*Department of Physics, Kyushu University, Fukuoka 819-0395, Japan*

<sup>2</sup>*Department of Physics, Niigata University, Niigata 950-2181, Japan*



(Received 18 November 2021; revised 17 September 2022; accepted 29 November 2022; published 14 February 2023)

**Background:** Very recently, the PREX and CREX collaborations presented skin values  $r_{\text{skin}}^{208}(\text{newPREX2}) = 0.278 \pm 0.078$  (exp)  $\pm 0.012$  (theor.) fm and  $r_{\text{skin}}^{48} = 0.121 \pm 0.026$  (exp)  $\pm 0.024$  (model), respectively. We recently determined a neutron-skin value  $r_{\text{skin}}^{208} = 0.278 \pm 0.035$  fm from measured reaction cross sections  $\sigma_{\text{R}}$  (exp) of  $p + ^{208}\text{Pb}$  scattering in a range of incident energies  $10 \lesssim E_{\text{in}} \lesssim 100$  MeV where the chiral (Kyushu)  $g$ -matrix folding model is reliable for  $^{12}\text{C} + ^{12}\text{C}$  scattering. The data  $\sigma_{\text{R}}$  (exp) are available for proton scattering on  $^{58}\text{Ni}$ ,  $^{40,48}\text{Ca}$ , and  $^{12}\text{C}$  targets.

**Purpose:** Our first aim is to test the Kyushu  $g$ -matrix folding model for  $p + ^{208}\text{Pb}$  scattering in  $20 \lesssim E_{\text{in}} \lesssim 180$  MeV. Our second aim is to determine skin values  $r_{\text{skin}}$  and matter and neutron radii,  $r_{\text{m}}$  and  $r_{\text{n}}$ , for  $^{208}\text{Pb}$ ,  $^{58}\text{Ni}$ ,  $^{40,48}\text{Ca}$ , and  $^{12}\text{C}$  from the  $\sigma_{\text{R}}$  (exp).

**Methods:** Our method is the Kyushu  $g$ -matrix folding model with the densities scaled from the D1S-GHFB+AMP densities, where D1S-GHFB+AMP stands for Gogny-D1S HFB (GHFB) with angular momentum projection (AMP).

**Results:** As for proton scattering, we find that our model is reliable in  $20 \lesssim E_{\text{in}} \lesssim 180$  MeV. For  $^{208}\text{Pb}$ , the skin value deduced from  $\sigma_{\text{R}}$  (exp) in  $20 \lesssim E_{\text{in}} \lesssim 180$  MeV is  $r_{\text{skin}}^{208}(\sigma_{\text{R}}) = 0.299 \pm 0.020$  fm. Our results on  $r_{\text{skin}}$  are compared with the previous works.

**Conclusion:** Our result  $r_{\text{skin}}^{208}(\sigma_{\text{R}}) = 0.299 \pm 0.020$  fm agrees with  $r_{\text{skin}}^{208}(\text{PREX2}) = 0.283 \pm 0.071$  fm. In addition, our result  $r_{\text{skin}}^{48} = 0.103 \pm 0.022$  fm is consistent with the CREX value.

DOI: [10.1103/PhysRevC.107.024608](https://doi.org/10.1103/PhysRevC.107.024608)

## I. INTRODUCTION

Many theoretical predictions on the symmetry energy  $S_{\text{sym}}(\rho)$  have been made so far by taking several experimental and observational constraints on  $S_{\text{sym}}(\rho)$  and their combinations. In a neutron star (NS), the  $S_{\text{sym}}(\rho)$  and its density ( $\rho$ ) dependence influence strongly the nature within the star. The symmetry energy  $S_{\text{sym}}(\rho)$  cannot be measured by experiment directly. In place of  $S_{\text{sym}}(\rho)$ , the neutron-skin thickness  $r_{\text{skin}}$  is measured to determine the slope parameter  $L$ , since a strong correlation between  $r_{\text{skin}}^{208}$  and  $L$  is well known [1].

Horowitz *et al.* [2] proposed a direct measurement for neutron-skin thickness  $r_{\text{skin}} = r_{\text{n}} - r_{\text{p}}$ , where  $r_{\text{n}}$  and  $r_{\text{p}}$  are the root-mean-square radii of neutrons and protons, respectively.

The PREX collaboration has reported a new value,

$$r_{\text{skin}}^{208}(\text{PREX2}) = 0.283 \pm 0.071 \text{ fm}, \quad (1)$$

combining the original Lead Radius EXperiment (PREX) result [3,4] with the updated PREX2 result [5]. Very recently, the PREX collaboration has presented an accurate value

$$\begin{aligned} r_{\text{skin}}^{208}(\text{newPREX2}) \\ = 0.278 \pm 0.078 \text{ (exp)} \pm 0.012 \text{ (theor.) fm}, \end{aligned} \quad (2)$$

The value is most reliable for  $^{208}\text{Pb}$ . The  $r_{\text{skin}}^{208}(\text{PREX2})$  value is considerably larger than the other experimental values that are significantly model dependent [6–9]. As an exceptional case, a nonlocal dispersive-optical-model (DOM) analysis of  $^{208}\text{Pb}$  deduces  $r_{\text{skin}}^{\text{DOM}} = 0.25 \pm 0.05$  fm [10] consistent with  $r_{\text{skin}}^{208}(\text{PREX2})$ .

Very recently, the CREX group has presented [11]

$$r_{\text{skin}}^{48}(\text{CREX}) = 0.121 \pm 0.026 \text{ (exp)} \pm 0.024 \text{ (model) fm}. \quad (3)$$

The CREX value is most reliable for  $^{48}\text{Ca}$ .

The  $r_{\text{skin}}^{208}(\text{PREX2})$  provides crucial tests for the equation of state (EoS) of nuclear matter [12–16]. For example, Reed *et al.* [17] report a value of the slope parameter  $L$  and examine the impact of such a stiff symmetry energy on some critical NS observables. They deduce

$$L = 106 \pm 37 = 69\text{--}143 \text{ MeV} \quad (4)$$

from  $r_{\text{skin}}^{208}(\text{PREX2})$ .

In Ref. [18], we accumulated the 206 EoSs from Refs. [1,19–43] in which  $r_{\text{skin}}^{208}$  and/or  $L$  is presented. The correlation between  $r_{\text{skin}}^{208}$  and  $L$  is more reliable when the number of EoSs is larger. The resulting relation

$$L = 620.39 r_{\text{skin}}^{208} - 57.963 \text{ MeV} \quad (5)$$

\*orion093g@gmail.com

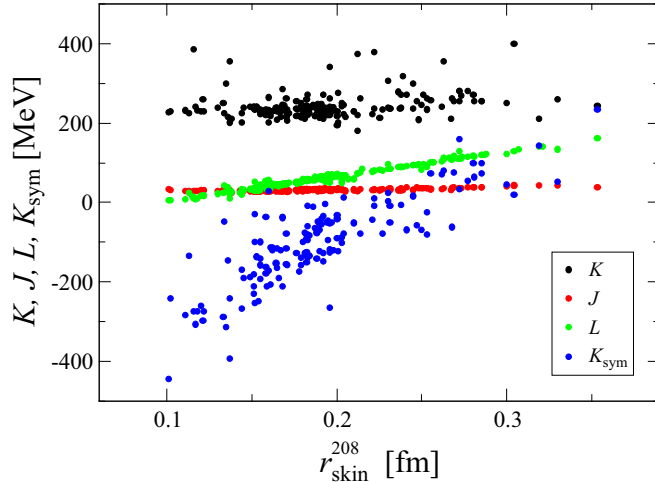


FIG. 1.  $r_{\text{skin}}^{208}$  dependence of  $J$ ,  $L$ , and  $K_{\text{sym}}$ , where  $J$ ,  $L$ , and  $K_{\text{sym}}$  are a constant term, the first-derivative term, and the second-derivative term of the symmetry energy. The dots show 206 EoSs taken from Table I of Ref. [18]. Obviously, the correlation between  $r_{\text{skin}}^{208}$  and  $L$  is linear.

has a strong correlation with the correlation coefficient  $R = 0.99$ , as shown in Fig. 1.

The relation (5) allows us to deduce a constraint on  $L$  from the PREX2 value. The resulting range of  $L$  is  $L = 76\text{--}165$  MeV, while the equation shown in Ref. [1] yields  $L = 76\text{--}172$  MeV. These values and  $L = 69\text{--}143$  MeV support stiffer EoSs. The stiffer EoSs allow us to consider phase transitions such as the QCD transition in an NS. The following EoSs satisfy  $L = 76\text{--}172$  MeV: SkO, FKVW, Rs, SV-sym34, es325, TFa, NL $\rho$ , BSR6, R $\sigma$ , Sk-Rs, E0009, Gs, Z271, GM3, PKDD, E0008(TMA), SK272, GM1, G $\sigma$ , Sk-T4, SK255, SV, es35, S271, SkI3, rG2, PC-PK1, SkI2, E0025, PC-LA, rNLC, E0036, rTM1, TM1, NL4, rNL-SH, NL-SH, rNL-RA1, PC-F2, PK1, PC-F1, NL3, rNL3, PC-F3, PC-F4, NL3\*, TFb, rNL3\*, SkI5, NL2, rNL-Z, TFc, NL1, rNL1, and SkI1 in Table I of Ref. [18].

As an indirect measurement, meanwhile, the high-resolution  $E1$  polarizability experiment ( $E1pE$ ) yields

$$r_{\text{skin}}^{208}(E1pE) = 0.156_{-0.021}^{+0.025} = 0.135\text{--}0.181 \text{ fm} \quad (6)$$

for  $^{208}\text{Pb}$  [8] and

$$r_{\text{skin}}^{48}(E1pE) = 0.17 \pm 0.03 = 0.14\text{--}0.20 \text{ fm} \quad (7)$$

for  $^{48}\text{Ca}$  [44].

TABLE I. Scaling factors  $\alpha_n$  and  $\alpha_p$  for neutron and proton.

	$\alpha_n$	$\alpha_p$
$^{208}\text{Pb}$	1.015	1.000
$^{58}\text{Ni}$	1.003	0.994
$^{48}\text{Ca}$	0.973	0.982
$^{40}\text{Ca}$	1.000	0.995
$^{12}\text{C}$	0.942	0.957

There is no overlap between  $r_{\text{skin}}^{208}(\text{PREX2})$  and  $r_{\text{skin}}^{208}(E1pE)$  in one  $\sigma$  level. However, we determined a value of  $r_{\text{skin}}^{208}(\text{exp})$  from measured reaction cross sections  $\sigma_R(\text{exp})$  of  $p + ^{208}\text{Pb}$  scattering in a range of incident energies,  $30 \lesssim E_{\text{in}} \lesssim 100$  MeV [45]; the value is  $r_{\text{skin}}^{208}(\text{exp}) = 0.278 \pm 0.035$  fm. Our result agrees with  $R_{\text{skin}}^{208}(\text{PREX2})$ . We also deduced  $r_n(\text{exp}) = 5.722 \pm 0.035$  fm and  $r_m(\text{exp}) = 5.614 \pm 0.022$  fm in addition to  $r_{\text{skin}}^{208}(\text{exp})$ . As for  $\text{He} + ^{208}\text{Pb}$  scattering, we determine  $r_{\text{skin}}^{208}(\text{exp}) = 0.416 \pm 0.146$  fm [46]. Our results are consistent with PREX II and therefore support a larger slope parameter  $L$ .

Our model is the chiral (Kyushu)  $g$ -matrix folding model with the densities calculated with Gogny-D1S HFB (D1S-GHFB) with angular momentum projection (AMP) [47,48]. For  $p + ^{208}\text{Pb}$  scattering, the neutron density is scaled so that the  $r_n$  of the scaled neutron density can reproduce the data [49–51] on  $\sigma_R$ , since the  $r_p$  of D1S-GHFB+AMP proton density agrees with the  $r_p(\text{exp})$  [52] determined from electron scattering. For  $^{12}\text{C}$  scattering on  $^9\text{Be}$ ,  $^{12}\text{C}$ , and  $^{27}\text{Al}$  targets, we tested reliability of the Kyushu  $g$ -matrix folding model and found that the Kyushu  $g$ -matrix folding model is reliable in  $30 \lesssim E_{\text{in}} \lesssim 100$  and  $250 \lesssim E_{\text{in}} \lesssim 400$  MeV [48]. This is the reason why we took  $30 \lesssim E_{\text{in}} \lesssim 100$  MeV in the analyses [45] of  $p + ^{208}\text{Pb}$  scattering. After the analyses, we find that the Kyushu  $g$ -matrix folding model reproduces the lower bound of the data on  $\sigma_R$  [53] for  $^{12}\text{C} + ^{12}\text{C}$  scattering at  $E_{\text{in}} = 10.4$  MeV per nucleon.

The  $g$ -matrix folding model is a standard way of deriving the microscopic optical potential for proton scattering and nucleus-nucleus scattering [47,48,54–62]. The folding model is composed of the single-folding model for proton scattering and the double-folding model for nucleus-nucleus scattering. The relation between the single- and the double-folding model is clearly shown in Ref. [59]. Applying the double-folding model based on the Melbourne  $g$  matrix [57] for the data [63] on interaction cross sections, we found that  $^{31}\text{Ne}$  is a halo nucleus with large deformation [62], and deduced the matter radii  $r_m$  for Ne isotopes [64]. Also for Mg isotopes, we determined the  $r_m$  from  $\sigma_R(\text{exp})$  for scattering of Mg isotopes on a  $^{12}\text{C}$  target [65].

Now, we consider proton scattering on  $^{208}\text{Pb}$ ,  $^{58}\text{Ni}$ ,  $^{40,48}\text{Ca}$ , and  $^{12}\text{C}$  targets, since there is no interaction cross section for proton scattering. In fact, good data on  $\sigma_R$  are available in Refs. [49–51] for  $^{208}\text{Pb}$ , Refs. [50,51,66–68] for  $^{58}\text{Ni}$ , Ref. [69] for  $^{48}\text{Ca}$ , Refs. [49–51] for  $^{40}\text{Ca}$ , and Refs. [50,51,70] for  $^{12}\text{C}$ . We have already shown that for  $p + ^{208}\text{Pb}$  scattering the  $\sigma_R$  calculated with  $r_{\text{skin}}^{208}(\text{PREX2})$  and  $r_p(\text{exp}) = 5.444$  fm [52] of electron scattering reproduce the data at  $E_{\text{lab}} = 534.1, 549,$  and  $806$  MeV [71].

In this paper, we first test the Kyushu  $g$ -matrix single-folding model for  $p + ^{208}\text{Pb}$  scattering, since the PREX2 data are available. We find that the present model is reliable in  $20 \lesssim E_{\text{in}} \lesssim 180$  MeV, as shown in Sec. III F. After the testing, we determine  $r_m(\text{exp})$ ,  $r_n(\text{exp})$ , and  $r_{\text{skin}}(\text{exp})$  for  $^{208}\text{Pb}$ ,  $^{58}\text{Ni}$ ,  $^{40,48}\text{Ca}$ , and  $^{12}\text{C}$  from the  $\sigma_R(\text{exp})$  in  $20 \lesssim E_{\text{in}} \lesssim 180$  MeV, as shown in Sec. III G. For each nucleus, the D1S-GHFB+AMP proton and neutron densities are scaled so as to reproduce  $\sigma_R(\text{exp})$  under the condition that the

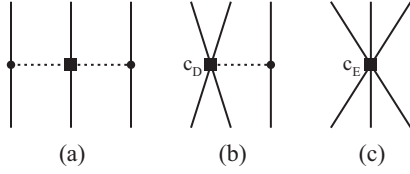


FIG. 2. 3NFs in NNLO (next-to-next-to-leading order). Diagram (a) corresponds to the Fujita-Miyazawa  $2\pi$ -exchange 3NF (next-to-next-to-next-to-leading order) [72], and diagrams (b) and (c) correspond to  $1\pi$ -exchange and contact 3NFs. The solid and dashed lines denote nucleon and pion propagations, respectively, and filled circles and squares stand for vertices. The strength of the filled-square vertex is often called  $c_D$  in diagram (b) and  $c_E$  in diagram (c).

$r_p$ (scaling) of the scaled proton density agrees with  $r_p$ (exp) of electron scattering.

We explain our model in Sec. II and our results in Sec. III. Section IV is devoted to a summary.

## II. MODEL

Our model is the Kyushu  $g$ -matrix folding model [47,48] with the proton and neutron densities scaled from the DIS-GHFB+AMP densities.

### A. The Kyushu $g$ -matrix folding model

Kohno calculated the  $g$  matrix for the symmetric nuclear matter, using the Brueckner-Hartree-Fock method with chiral  $N^3$ LO 2NFs and NNLO 3NFs [73], where  $N^3$ LO 3NF is the abbreviation of next-to-next-to-next-to-leading-order three-body force and NNLO 2NFs is the abbreviation of next-to-next-to-leading-order two-body force. He set  $c_D = -2.5$  and  $c_E = 0.25$  so that the energy per nucleon can become minimum at  $\rho = \rho_0$ ; see Fig. 2 for the definition of  $c_D$  and  $c_E$ . Toyokawa *et al.* localized the nonlocal chiral  $g$  matrix into three-range Gaussian forms [47], using the localization method proposed by the Melbourne group [57,74,75]. The resulting local  $g$  matrix is referred to as the ‘‘Kyushu  $g$  matrix.’’ The Kyushu  $g$  matrix is constructed from chiral interaction with the cutoff 550 MeV.

The Kyushu  $g$ -matrix folding model is successful in reproducing  $\sigma_R$ , differential cross sections  $d\sigma/d\Omega$ , and vector analyzing powers  $A_y$  for  $^4\text{He}$  scattering in  $E_{\text{in}} = 30\text{--}200$  MeV per nucleon [47]. The model is successful for proton scattering at  $E_{\text{in}} = 65$  MeV [60].

In Ref. [48], we tested the Kyushu  $g$ -matrix folding model [47] for  $^{12}\text{C}$  scattering on  $^9\text{Be}$ ,  $^{12}\text{C}$ , and  $^{27}\text{Al}$  targets in  $30 \lesssim E_{\text{in}} \lesssim 400$  MeV. We found that the Kyushu  $g$ -matrix folding model is reliable for  $\sigma_R$  in  $30 \lesssim E_{\text{in}} \lesssim 100$  and  $250 \lesssim E_{\text{in}} \lesssim 400$  MeV. This indicates that the Kyushu  $g$ -matrix folding model is applicable in the  $E_{\text{in}}$  range. After the test, we found that our model reproduces the lower bound of measured reaction cross section  $\sigma_R$  [53] at  $E_{\text{in}} = 10.4$  MeV. Our model is reliable for  $10 \lesssim E_{\text{in}} \lesssim 100$  MeV and  $250 \lesssim E_{\text{in}} \lesssim 400$  MeV.

We recapitulate the single-folding model for nucleon-nucleus scattering. The potential  $U(\mathbf{R})$  consists of the direct and exchange parts [59],  $U^{\text{DR}}(\mathbf{R})$  and  $U^{\text{EX}}(\mathbf{R})$ , defined by

$$U^{\text{DR}}(\mathbf{R}) = \sum_{\mu,\nu} \int \rho_T^{\nu}(\mathbf{r}_T) g_{\mu\nu}^{\text{DR}}(s; \rho_{\mu\nu}) d\mathbf{r}_T, \quad (8a)$$

$$U^{\text{EX}}(\mathbf{R}) = \sum_{\mu,\nu} \int \rho_T^{\nu}(\mathbf{r}_T, \mathbf{r}_T + s) \times g_{\mu\nu}^{\text{EX}}(s; \rho_{\mu\nu}) \exp[-i\mathbf{K}(\mathbf{R}) \cdot s/M] d\mathbf{r}_T, \quad (8b)$$

where  $\mathbf{R}$  is the relative coordinate between a projectile ( $P$ ) and a target ( $T$ ),  $s = -\mathbf{r}_T + \mathbf{R}$ , and  $\mathbf{r}_T$  is the coordinate of the interacting nucleon from the center of mass of  $T$ . Each of  $\mu$  and  $\nu$  denotes the  $z$  component of isospin, i.e.,  $(1/2, -1/2)$  corresponds to (neutron, proton). The nonlocal  $U^{\text{EX}}$  has been localized in Eq. (8b) with the local semiclassical approximation [54], where  $K(R)$  is the local momentum between  $P$  and  $T$ , and  $M = A/(1+A)$  for the target mass number  $A$ ; see Ref. [76] for the validity of the localization. The direct and exchange parts,  $g_{\mu\nu}^{\text{DR}}$  and  $g_{\mu\nu}^{\text{EX}}$ , of the  $g$  matrix depend on the local density

$$\rho_{\mu\nu} = \sigma^{\mu} \rho_T^{\nu}(\mathbf{r}_T + s/2) \quad (9)$$

at the midpoint of the interacting nucleon pair, where  $\sigma^{\mu}$  having  $\mu = -1/2$  is the Pauli matrix of an incident proton. As a way of taking the center-of-mass correction to the DIS-GHFB+AMP densities, we use the method of Ref. [64], since the procedure is quite simple.

The direct and exchange parts,  $g_{\mu\nu}^{\text{DR}}$  and  $g_{\mu\nu}^{\text{EX}}$ , of the  $g$  matrix are described by [64]

$$\begin{aligned} & g_{\mu\nu}^{\text{DR}}(s; \rho_{\mu\nu}) \\ &= \begin{cases} \frac{1}{4} \sum_S \hat{S}^2 g_{\mu\nu}^{S1}(s; \rho_{\mu\nu}); & \text{for } \mu + \nu = \pm 1 \\ \frac{1}{8} \sum_{S,T} \hat{S}^2 g_{\mu\nu}^{ST}(s; \rho_{\mu\nu}); & \text{for } \mu + \nu = 0 \end{cases} \quad (10) \\ & g_{\mu\nu}^{\text{EX}}(s; \rho_{\mu\nu}) \\ &= \begin{cases} \frac{1}{4} \sum_S (-1)^{S+1} \hat{S}^2 g_{\mu\nu}^{S1}(s; \rho_{\mu\nu}); & \text{for } \mu + \nu = \pm 1 \\ \frac{1}{8} \sum_{S,T} (-1)^{S+T} \hat{S}^2 g_{\mu\nu}^{ST}(s; \rho_{\mu\nu}); & \text{for } \mu + \nu = 0 \end{cases} \quad (11) \end{aligned}$$

where  $\hat{S} = \sqrt{2S+1}$  and  $g_{\mu\nu}^{ST}$  are the spin-isospin components of the  $g$  matrix; see Ref. [47] for the explicit form of  $g_{\mu\nu}^{\text{DR}}$  and  $g_{\mu\nu}^{\text{EX}}$ .

The potential  $U(\mathbf{R})$  thus obtained has the form of  $U(\mathbf{R}) = U_{\text{cent}}(\mathbf{R}) + \hat{\ell} \cdot \hat{\sigma} U_{\text{spin-orbit}}(\mathbf{R})$ , where  $U_{\text{cent}}(\mathbf{R})$  and  $U_{\text{spin-orbit}}(\mathbf{R})$  are the central and the spin-orbit part of  $U(\mathbf{R})$ , respectively, and  $\ell$  is the orbital angular momentum of the proton scattering; see Eq. (28) in Ref. [64] for the derivation. The relative wave function  $\psi$  between  $P$  and  $T$  can be decomposed into partial waves  $\chi_{\ell}$ , each with different  $\ell$ . The  $\chi_{\ell}$  is obtained by solving the Schrödinger equation having  $U(\mathbf{R})$ . The elastic  $S$ -matrix elements  $S_{\ell}$  are obtained from the asymptotic form of  $\chi_{\ell}$ . The total reaction cross section  $\sigma_R$  is calculable from the  $S_{\ell}$  as

$$\sigma_R = \frac{\pi}{K^2} \sum_{\ell} (2\ell + 1)(1 - |S_{\ell}|^2). \quad (12)$$

TABLE II. Fine-tuning factor  $F$ .

	$F$
$^{208}\text{Pb}$	1
$^{58}\text{Ni}$	0.96473
$^{48}\text{Ca}$	0.9810
$^{40}\text{Ca}$	0.92716
$^{12}\text{C}$	0.93077

### B. Scaling procedure of proton and neutron densities

The proton and neutron densities,  $\rho_p(r)$  and  $\rho_n(r)$ , are scaled from the D1S-GHFB+AMP densities. We can obtain the scaled density  $\rho_{\text{scaling}}(\mathbf{r})$  from the original density  $\rho(\mathbf{r})$  as

$$\rho_{\text{scaling}}(\mathbf{r}) = \frac{1}{\alpha^3} \rho(\mathbf{r}/\alpha) \quad (13)$$

with a scaling factor

$$\alpha = \sqrt{\frac{\langle r^2 \rangle_{\text{scaling}}}{\langle r^2 \rangle}}. \quad (14)$$

For later convenience, we refer to the proton (neutron) radius of the scaled proton (neutron) density  $\rho_{\text{scaling}}^p(\mathbf{r})$  [ $\rho_{\text{scaling}}^n(\mathbf{r})$ ] as  $r_p(\text{scaling})$  [ $r_n(\text{scaling})$ ].

Table II shows the scaling factors,  $\alpha_p$  and  $\alpha_n$ , from the D1S-GHFB+AMP densities to the scaled densities that reproduce data  $\sigma_R(\text{exp})$  and  $r_p(\text{exp})$  of electron scattering.

### C. Effective nucleon-nucleon interaction for targets

For a change of the proton and neutron distributions in targets, a microscopic approach is to modify D1S. For the Gogny EoSs, the effective nucleon-nucleon interaction can be described as

$$\begin{aligned} V(\vec{r}) = & \sum_{i=1,2} t_0^i (1 + x_0^i P_\sigma) \rho^{\alpha_i} \delta(\vec{r}) \\ & + \sum_{i=1,2} (W_i + B_i P_\sigma - H_i P_\tau - M_i P_\sigma P_\tau) e^{-\frac{r^2}{\mu_i^2}} \\ & + iW_0(\sigma_1 + \sigma_2) [\vec{k}' \times \delta(\vec{r}) \vec{k}], \end{aligned} \quad (15)$$

where  $\sigma$  and  $\tau$  are the Pauli spin and isospin operators, respectively, and the corresponding exchange operators  $P_\sigma$  and  $P_\tau$  are defined as usual.

For  $^{208}\text{Pb}$ , we have changed all parameters of D1S, but cannot find the NN interaction that reproduces  $r_{\text{skin}}^{208}(\text{PREX2}) = 0.283 \pm 0.071$  fm. The best fitting is the D1PK2-GHFB+AMP with  $r_{\text{skin}}^{208}(\text{D1PK2}) = 0.185$  fm; note that  $r_{\text{skin}}^{208}(\text{D1S}) = 0.137$  fm. The parameters of D1PK2 are shown in Table III.

TABLE III. Parameter sets of D1PK2.

D1PK	$\mu_i$	$W_i$	$B_i$	$H_i$	$M_i$	$t_0^i$	$x_0^i$	$\alpha_i$	$W_0$
$i = 1$	0.90	-465.027582	155.134492	-506.775323	117.749903	981.065351	1	1/3	130
$i = 2$	1.44	34.6200000	-14.0800000	70.9500000	-41.3518104	534.155654	-1	1	

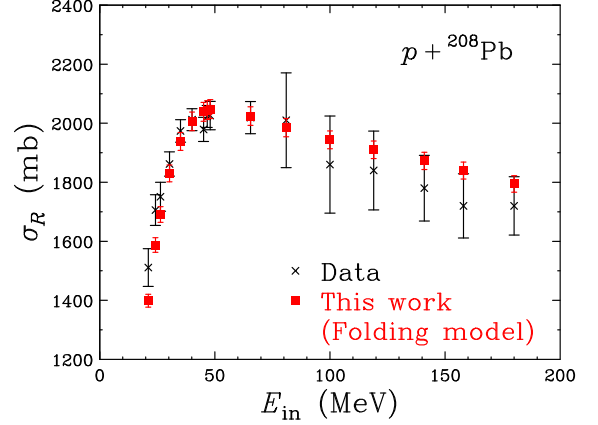


FIG. 3.  $E_{\text{in}}$  dependence of reaction cross sections  $\sigma_R$  for  $p + ^{208}\text{Pb}$  scattering. The squares with error bar (legend “This work (Folding model)”) stand for the results of the folding model with the densities scaled to PREX2, whereas the crosses with error bar correspond to the data [49–51] on  $\sigma_R$ .

## III. RESULTS

First of all, we regard reliable  $r_m$  and  $r_n$  as reference values,  $r_m(\text{ref})$  and  $r_n(\text{ref})$ , in order to determine  $r_m(\text{exp})$  from  $\sigma_R(\text{exp})$ . The reference values are shown below; see Table IV for the numerical values. Whenever we calculate  $\sigma_R$ , we use the Kyushu  $g$ -matrix model.

### A. $^{58}\text{Ni}$

The reference values are the  $r_m(\text{AMP})$  and  $r_n(\text{AMP})$  calculated with D1S-GHFB+AMP, since the  $\sigma_R(\text{AMP})$  are near the upper bound of the data, as shown in Fig. 5.  $E_{\text{in}}$  dependence of  $\sigma_R(\text{AMP})$  is similar to that of the data. We then define the ratio  $F(E_{\text{in}}) \equiv \sigma_R(\text{exp})/\sigma_R(\text{ref}) = \sigma_R(\text{exp})/\sigma_R(\text{AMP})$ , and introduce the average value of  $F(E_{\text{in}})$  as a fine-tuning factor  $F$ . The factor is  $F = 0.96473$  close to 1. The  $F\sigma_R(\text{AMP})$  almost reproduce the central values of the data, as shown in Fig. 5. The scaling procedure is not made to get the reference values, i.e.,  $\alpha = 1$ .

### B. $^{208}\text{Pb}$

The reference values are the  $r_m(\text{PREX2})$  and  $r_n(\text{PREX2})$  evaluated from  $r_{\text{skin}}^{208}(\text{PREX2})$  and  $r_p(\text{exp})$  [52] of electron scattering. In this case, the  $\sigma_R(\text{exp})$  based on the densities scaled to  $r_n(\text{PREX2})$  and  $r_p(\text{exp})$  reproduce the data within the error bar, as shown in Fig. 3. For this reason,  $F$  is 1.

TABLE IV. Reference values of  $r_m(\text{ref})$ ,  $r_n(\text{ref})$ , and  $r_{\text{skin}}(\text{ref})$  together with  $r_p(\text{exp})$  of electron scattering. The  $r_p(\text{exp})$  are deduced from the electron scattering [52,77]. In actual calculations, the central values are taken as reference values. The radii are shown in units of fm.

	Ref.	$r_p(\text{exp})$	$r_m(\text{ref})$	$r_n(\text{ref})$	$r_{\text{skin}}(\text{ref})$
$^{208}\text{Pb}$	PREX2	5.444	$5.617 \pm 0.044$	$5.727 \pm 0.071$	$0.283 \pm 0.071$
$^{58}\text{Ni}$	D1S AMP	3.727	3.721	3.715	-0.013
$^{48}\text{Ca}$	CREX	3.385	$3.456 \pm 0.050$	$3.506 \pm 0.050$	$0.121 \pm 0.050$
$^{40}\text{Ca}$	[78]	3.385	$3.380^{+0.022}_{-0.023}$	$3.375^{+0.022}_{-0.023}$	$-0.010^{+0.022}_{-0.023}$
$^{12}\text{C}$	[79]	2.327	$2.35 \pm 0.02$	$2.37 \pm 0.02$	$0.05 \pm 0.02$

### C. $^{48}\text{Ca}$

We can obtain  $r_m(\text{CREX})$  and  $r_n(\text{CREX})$  from the CREX value of Eq. (3) and  $r_p(\text{exp}) = 3.385$  fm [77] of electron scattering. In this case, the  $\sigma_R(\text{CREX})$  based on  $r_n(\text{CREX})$  and  $r_p(\text{exp})$  are near the central values of of the data, as shown in Fig. 6. The fine-tuning factor is  $F = 0.9810$  close to 1. The  $F\sigma_R(E \text{ 1pE})$  almost reproduce the central values of the data, as shown in Fig. 6.

### D. $^{40}\text{Ca}$

As for  $^{40,48}\text{Ca}$ , Zenihiro *et al.* measured the differential cross section and the analyzing powers for  $p + ^{40,48}\text{Ca}$  scattering in Research Center for Nuclear Physics (RCNP), and determined  $r_{\text{skin}}^{40,48}(\text{RCNP})$  [78]. For  $^{48}\text{Ca}$ , the value  $r_{\text{skin}}(\text{RCNP}) = 0.168^{+0.025}_{-0.028}$  fm is consistent with  $r_{\text{skin}}^{48}(E \text{ 1pE})$ . For  $^{40}\text{Ca}$ , their values are shown in Table IV as reference values. Since  $\sigma_R(\text{RCNP}) = \sigma_R(\text{AMP})$ , the  $\sigma_R(\text{AMP})$  are reliable. In this case, the  $\sigma_R(\text{AMP})$  overshoot the data, as shown in Fig. 7. The fine-tuning factor is  $F = 0.92716$  close to 1. The  $F\sigma_R(\text{AMP})$  almost reproduce the central values of the data, as shown in Fig. 7.

### E. $^{12}\text{C}$

Tanihata *et al.* measured interaction cross sections at 790 MeV/nucleon in GSI Helmholtzzentrum für Schwerionenforschung GmbH (GSI) and determined  $r_m(\text{GSI}) = 2.35$  fm for  $^{12}\text{C}$  [79]. The  $r_m(\text{GSI})$  and  $r_p(\text{exp}) = 2.327$  fm [77] lead to  $r_n(\text{GSI}) = 2.37$  fm. The  $r_m(\text{GSI})$  and  $r_n(\text{GSI})$  are reference values. The fine-tuning factor is  $F = 0.93077$  close to 1. The  $F\sigma_R(\text{GSI})$  are near the central values of  $\sigma_R(\text{exp})$ , as shown in Fig. 8.

When we determine  $r_m(\text{exp})$  from data  $\sigma_R(\text{exp})$ , we scale the D1S-GHFB+AMP proton and neutron densities so as to obtain  $F\sigma_R(\text{ref}) = \sigma_R(\text{exp})$  and  $r_p(\text{scaling}) = r_p(\text{exp})$ . Next, we deduce  $r_m(\text{exp})$  from  $r_n(\text{scaling})$  and  $r_p(\text{scaling})$  for each  $E_{\text{in}}$ . The resulting  $r_m(\text{exp})$  depends on  $E_{\text{in}}$ . For all the  $r_m(\text{exp})$ , we take the weighted mean and its error. Finally, we evaluate  $r_{\text{skin}}(\text{exp})$  and  $r_n(\text{exp})$  from the resulting  $r_m(\text{exp})$  and the  $r_p(\text{exp})$  [52,77] of the electron scattering. For later convenience, we refer to this procedure as ‘‘experimental scaling procedure with  $F$  (ESP-F)’’.

### F. Test of the Kyushu $g$ -matrix folding model for $p + ^{208}\text{Pb}$ scattering

Now we test the Kyushu  $g$ -matrix model for proton scattering. As shown in Fig. 3, the  $\sigma_R$  (squares with error bar) based

on  $R_{\text{skin}}^{208}(\text{PREX2})$  and  $r_p(\text{exp})$  are consistent with data [49–51] in  $20 \lesssim E_{\text{in}} \lesssim 180$  MeV; see Table IV for  $R_{\text{skin}}^{208}(\text{PREX2})$  and  $r_p(\text{exp})$ . This indicates that our model is good in  $20 \lesssim E_{\text{in}} \lesssim 180$  MeV for proton scattering.

### G. $^{208}\text{Pb}$ , $^{58}\text{Ni}$ , $^{48,40}\text{Ca}$ , and $^{12}\text{C}$

#### 1. $^{208}\text{Pb}$

Figure 4 shows reaction cross sections  $\sigma_R$  of  $p + ^{208}\text{Pb}$  scattering as a function of  $E_{\text{in}}$ . The results of the D1S-GHFB+AMP densities reproduce the data [49–51] with 4% errors. This is true for the neutron density scaled to the central value of PREX2 and the D1S-GHFB+AMP density. In the results of the Woods-Saxon type neutron density ( $r_{\text{WS}} = 6.59$  fm,  $a_{\text{WS}} = 0.7$  fm) fitted to the central value of PREX2, we use the D1S-GHFB+AMP proton density. The results of the Woods-Saxon type neutron density ( $r_{\text{WS}} = 6.59$  fm,  $a_{\text{WS}} = 0.7$  fm) and the D1S-GHFB+AMP proton density are close to those of the neutron density scaled to the central value of PREX2 and the D1S-GHFB+AMP proton density. The Woods-Saxon type neutron density ( $r_{\text{WS}} = 6.81$  fm,  $a_{\text{WS}} = 0.6$  fm) yields almost the same results as the case of  $r_{\text{WS}} = 6.59$  fm,  $a_{\text{WS}} = 0.7$  fm, that is, the former undershoots the

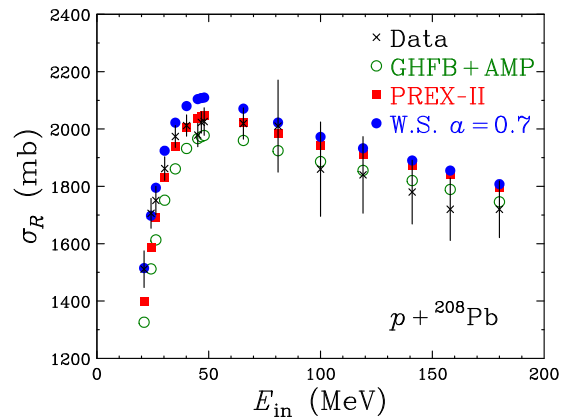


FIG. 4.  $E_{\text{in}}$  dependence of reaction cross sections  $\sigma_R$  for  $p + ^{208}\text{Pb}$  scattering. Squares stand for the results of the folding model with the neutron density scaled to the central value of PREX2. Open circles denote the results of the D1S-GHFB+AMP densities, and close circles correspond to the results of the Woods-Saxon type neutron density ( $r_{\text{WS}} = 6.59$  fm,  $a_{\text{WS}} = 0.7$  fm) fitted to the central value of PREX2. As for the proton density, it is calculated with D1S-GHFB+AMP for three types of calculations. The crosses with error bar are the data [49–51] on  $\sigma_R$ .

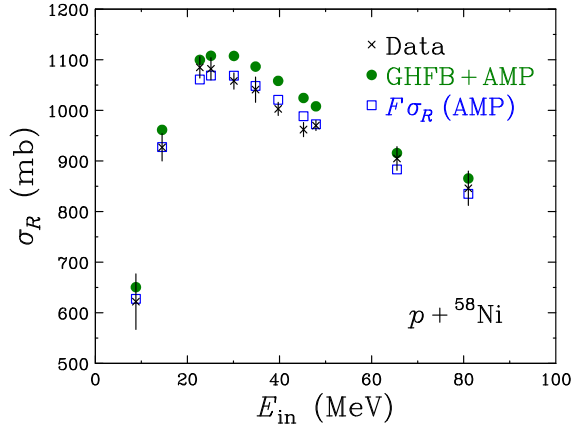


FIG. 5.  $E_{in}$  dependence of reaction cross sections  $\sigma_R$  for  $p + {}^{58}\text{Ni}$  scattering. Closed circles denote results of the D1S-GHFB+AMP densities. Squares stand for  $F\sigma_R(\text{AMP})$  with  $F = 0.96473$ . The data (crosses) are taken from Refs. [50,51,66–68].

latter by 0.974. We then do not show the former results in Fig. 4.

The results of ESP-F are  $r_{\text{skin}}^{208}(\text{exp}) = 0.299 \pm 0.020$  fm,  $r_n(\text{exp}) = 5.743 \pm 0.020$  fm,  $r_m(\text{exp}) = 5.627 \pm 0.020$  fm. The present skin value  $0.299 \pm 0.020$  fm almost agrees with our previous value  $r_{\text{skin}}^{208}(\text{exp}) = 0.278 \pm 0.035$  fm of Ref. [45].

### 2. ${}^{58}\text{Ni}$

Figure 5 shows  $\sigma_R$  as a function of  $E_{in}$  for  $p + {}^{58}\text{Ni}$  scattering. The results  $\sigma_R(\text{AMP})$  of the Kyushu  $g$ -matrix folding model with the D1S-GHFB+AMP densities (closed circles) almost reproduce data  $\sigma_R(\text{exp})$  [50,51,66–68] in  $10 \lesssim E_{in} \lesssim 81$  MeV; note that the data have a high accuracy of 2.7%.

The result of ESP-F is  $r_m(\text{exp}) = 3.711 \pm 0.010$  fm. Using the  $r_m(\text{exp})$  and  $r_p(\text{exp}) = 3.685$  fm [77], we can obtain  $r_{\text{skin}} = 0.055 \pm 0.010$  fm and  $r_n = 3.740 \pm 0.010$  fm.

A novel method for measuring nuclear reactions in inverse kinematics with stored ion beams was successfully used to extract the matter radius of  ${}^{58}\text{Ni}$  [80]. The experiment was performed at the experimental heavy-ion storage ring at the GSI facility. Their results determined from the differential cross section for  ${}^{58}\text{Ni} + {}^4\text{He}$  scattering are  $r_m(\text{GSI}) = 3.70(7)$  fm,  $r_p(\text{GSI}) = 3.68$  fm,  $r_n(\text{GSI}) = 3.71(12)$  fm, and  $r_{\text{skin}}(\text{GSI}) = 0.03(12)$  fm.

### 3. ${}^{48}\text{Ca}$

Figure 6 shows  $\sigma_R$  as a function of  $E_{in}$  for  $p + {}^{48}\text{Ca}$  scattering. The  $\sigma_R(\text{AMP})$  almost reproduce the data [69]. The results  $\sigma_R(\text{CREX})$  based on  $r_n(\text{CREX})$  and  $r_p(\text{exp})$  [77] are near the central values of the data [69].  $E_{in}$  dependence of  $\sigma_R(E_{1pE})$  is similar to that of the data [69]. The  $F\sigma_R(\text{CREX})$  almost reproduce the central values of the data.

The results of ESP-F are  $r_{\text{skin}} = 0.103 \pm 0.022$  fm and  $r_n = 3.488 \pm 0.022$  fm. Our skin value agrees with  $r_{\text{skin}}^{48}(\text{CREX})$ .

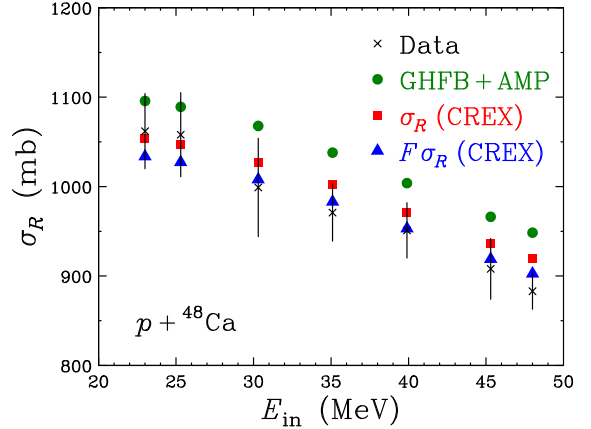


FIG. 6.  $E_{in}$  dependence of reaction cross sections  $\sigma_R$  for  $p + {}^{48}\text{Ca}$  scattering. Circles denote results of the D1S-GHFB+AMP densities, and squares correspond to the results of the scaled densities based on  $r_{\text{skin}}^{48}(\text{CREX})$ . Triangles stand for  $F\sigma_R(\text{CREX})$  with  $F = 0.9810$ . The data (crosses) are taken from Ref. [69].

### 4. ${}^{40}\text{Ca}$

Figure 7 shows  $\sigma_R$  as a function of  $E_{in}$  for  $p + {}^{40}\text{Ca}$  scattering. The Kyushu  $g$ -matrix folding model with the D1S-GHFB+AMP densities overestimates  $\sigma_R(\text{exp})$  [49–51]; note that the data have a high accuracy of 2.7%. Note that  $\sigma_R(\text{AMP}) = \sigma_R(\text{PCNP})$ , since  $r_m(\text{AMP})$  is very close to  $r_m(\text{RCNP})$ .  $E_{in}$  dependence of  $\sigma_R(\text{AMP})$  is similar to that of the data [49–51].

The result of ESP-F is  $r_m(\text{exp}) = 3.372 \pm 0.011$  fm. Using the  $r_m(\text{exp})$  and  $r_p(\text{exp}) = 3.378$  fm of electron scattering, we can obtain  $r_{\text{skin}}(\text{exp}) = -0.011 \pm 0.011$  fm and  $r_n(\text{exp}) = 3.367 \pm 0.011$  fm. Our results are close to those shown in Ref. [78]; see Table IV for the values of Ref. [78].

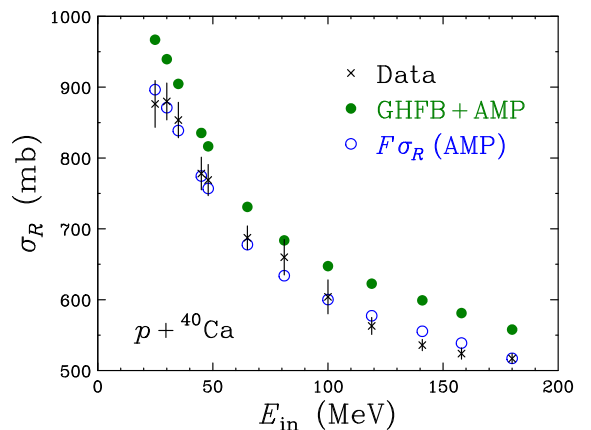


FIG. 7.  $E_{in}$  dependence of reaction cross sections  $\sigma_R$  for  $p + {}^{40}\text{Ca}$  scattering. Closed circles denote results of the original (D1S-GHFB+AMP) densities and the scaled ones, Open circles correspond to  $F\sigma_R(\text{AMP})$ . The data (crosses) are taken from Refs. [49–51].

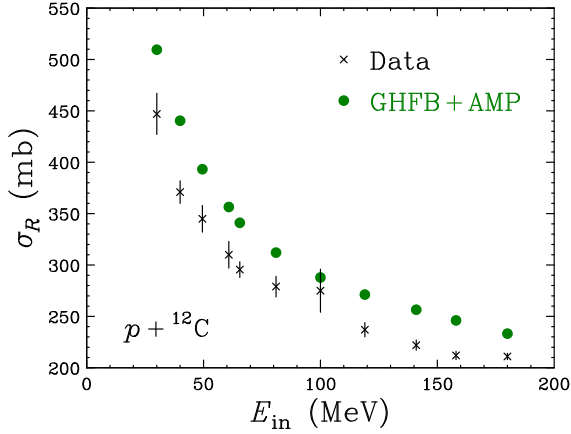


FIG. 8.  $E_{in}$  dependence of reaction cross sections  $\sigma_R$  for  $p + {}^{12}\text{C}$  scattering. Closed circles denote results  $F\sigma_R(\text{AMP})$ . The data (crosses) are taken from Refs. [50,51,70].

### 5. ${}^{12}\text{C}$

Figure 8 shows  $\sigma_R$  as a function of  $E_{in}$  for  $p + {}^{12}\text{C}$  scattering. The results  $\sigma_R(\text{AMP})$  of D1S-GHFB+AMP overshoot data  $\sigma_R(\text{exp})$  [50,51,70].

Figure 9 shows  $\sigma_R(\text{GSI})$  based on  $r_m(\text{GSI})$  and  $r_p(\text{exp}) = 2.327$  fm of electron scattering for  $p + {}^{12}\text{C}$  scattering. The results  $\sigma_R(\text{GSI})$  are near the upper bound of  $\sigma_R(\text{exp})$  [50,51,70]. The  $F\sigma_R(\text{GSI})$  (open circles) are near the central values of  $\sigma_R(\text{exp})$ .

The result of ESP-F is  $r_m(\text{exp}) = 2.340 \pm 0.009$  fm. Using the  $r_m(\text{exp})$  and  $r_p(\text{exp}) = 2.327$  fm, we can obtain  $r_{\text{skin}}(\text{exp}) = 0.026 \pm 0.009$  fm and  $r_n(\text{exp}) = 2.354 \pm 0.009$  fm.

Tanihata *et al.* determined  $r_m$  from interaction cross sections for He, Li, Be, and B isotopes [79]. In Ref. [81], the experimental values of  $r_m$  are accumulated from  ${}^4\text{He}$  to  ${}^{32}\text{Mg}$ . Our result  $r_m(\text{exp}) = 2.340 \pm 0.009$  fm is slightly smaller than  $r_m(\text{GSI}) = 2.35(2)$  fm. As for neutron radius, this is

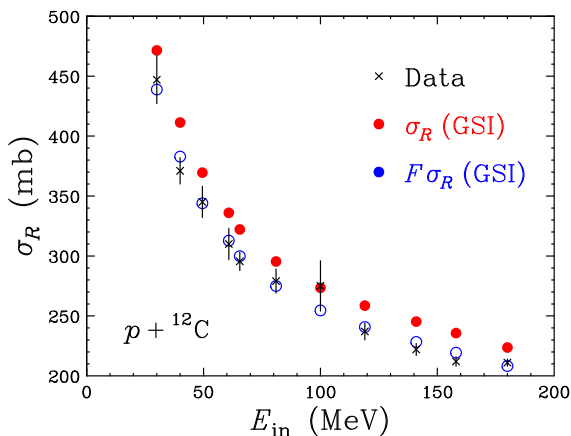


FIG. 9.  $E_{in}$  dependence of reaction cross sections  $\sigma_R$  for  $p + {}^{12}\text{C}$  scattering. Closed circles denote results  $\sigma_R(\text{GSI})$ , while open circles correspond to  $F\sigma_R(\text{GSI})$ . The data (crosses) are taken from Refs. [50,51,70].

TABLE V. Our results for  $r_m$ ,  $r_n$ , and  $r_{\text{skin}}$ . The radii are shown in units of fm.

	$r_m(\sigma_R)$	$r_n(\sigma_R)$	$r_{\text{skin}}(\sigma_R)$
${}^{208}\text{Pb}$	$5.627 \pm 0.020$	$5.743 \pm 0.020$	$0.299 \pm 0.020$
${}^{58}\text{Ni}$	$3.711 \pm 0.010$	$3.740 \pm 0.010$	$0.055 \pm 0.010$
${}^{48}\text{Ca}$	$3.445 \pm 0.022$	$3.488 \pm 0.022$	$0.103 \pm 0.022$
${}^{40}\text{Ca}$	$3.372 \pm 0.011$	$3.367 \pm 0.011$	$-0.011 \pm 0.011$
${}^{12}\text{C}$	$2.340 \pm 0.009$	$2.354 \pm 0.009$	$0.026 \pm 0.009$

the case because  $r_n(\text{exp}) = 2.354 \pm 0.009$  fm and  $r_n(\text{GSI}) = 2.37(2)$  fm.

## IV. SUMMARY

In this paper, we consider the  ${}^{208}\text{Pb}$ ,  ${}^{58}\text{Ni}$ ,  ${}^{40,48}\text{Ca}$ , and  ${}^{12}\text{C}$  as stable nuclei and determine  $r_{\text{skin}}(\sigma_R)$ ,  $r_m(\sigma_R)$ , and  $r_n(\sigma_R)$  from measured  $\sigma_R$ . Our results on  $r_{\text{skin}}(\sigma_R)$ ,  $r_m(\sigma_R)$ , and  $r_n(\sigma_R)$  are summarized in Table V. Comparing Table V with Table IV, we find that our results are close to the reference values.

We show mass-number ( $A$ ) dependence of stable nuclei in Figs. 10–12. Figure 10 shows skin values as a function of  $S_p - S_n$ , where  $S_p$  ( $S_n$ ) is the proton (neutron) separation energy. The skin values  $r_{\text{skin}}(\sigma_R)$  determined from measured  $\sigma_R$  for  ${}^{208}\text{Pb}$ ,  ${}^{58}\text{Ni}$ , and  ${}^{40,48}\text{Ca}$  are compared with the data of PREX2 [5],  ${}^{116,118,120,122,124}\text{Sn}$  [82,83], and  ${}^{48}\text{Ca}$  [44]. Our results are consistent with the previous experimental skin values.

Figure 11 shows matter radii  $r_m$  as a function of  $A^{1/3}$ . For  ${}^{208}\text{Pb}$ ,  ${}^{116,118,120,122,124}\text{Sn}$ , and  ${}^{48}\text{Ca}$ , the  $r_m$  are derived from the corresponding skin values [5,44,82,83] and the corre-

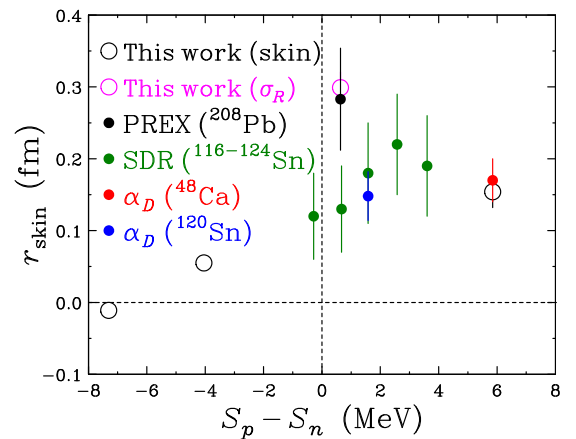


FIG. 10. Skin values as a function of  $S_p - S_n$ . The skin values determined from measured  $\sigma_R$  are shown with “This work (skin)” for  ${}^{208}\text{Pb}$  and with “This work ( $\sigma_R$ )” for  ${}^{58}\text{Ni}$  and  ${}^{40,48}\text{Ca}$ . The symbol “ $\alpha_D$ ” means the results of the  $E1$  polarizability experiment ( $E1pE$ ) for  ${}^{120}\text{Sn}$  [83] and  ${}^{48}\text{Ca}$  [44]. The symbol “PREX” stands for the result deduced from  $r_{\text{skin}}^{208}(\text{PREX2}) = 0.283 \pm 0.071$  fm. Open circles stand for the results of this paper. The symbol “SDR” shows the results [82] of the measurement based on the isovector spin-dipole resonances (SDR) in Sn isotopes. The data (closed circles with error bar) are taken from Refs. [5,44,82,83].

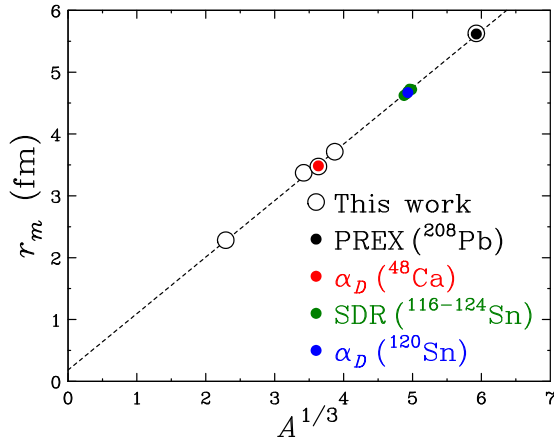


FIG. 11. Matter radii  $r_m$  as a function of mass number  $A^{1/3}$ . The symbol “ $\alpha_D$ ” means the results of the  $E1$  polarizability experiment ( $E1pE$ ) for  $^{120}\text{Sn}$  [83] and  $^{48}\text{Ca}$  [44]. The symbol “PREX” stands for the result deduced from  $r_{\text{skin}}^{208}$  (PREX2) =  $0.283 \pm 0.071$  fm. The symbol “SDR” shows the results [82] of the measurement based on the isovector spin-dipole resonances (SDR) in the Sb isotopes. Open circles stand for the results of this paper. The dashed line is a guide for the eyes. The data (closed circles with error bar) are taken from Refs. [5,44,82,83].

sponding  $r_p$  of electron scattering. For  $^{12}\text{C}$ ,  $^{40,48}\text{Ca}$ ,  $^{58}\text{Ni}$ , and  $^{208}\text{Pb}$ , our results are added. Our results are consistent with the previous works.

Figure 12 shows neutron radii  $r_n$  as a function of mass number  $A^{1/3}$ . For  $^{208}\text{Pb}$ ,  $^{116,118,120,122,124}\text{Sn}$ , and  $^{48}\text{Ca}$ , the  $r_n$  are derived from the corresponding skin values [5,44,82,83] and the corresponding  $r_p$  of electron scattering. For  $^{12}\text{C}$ ,

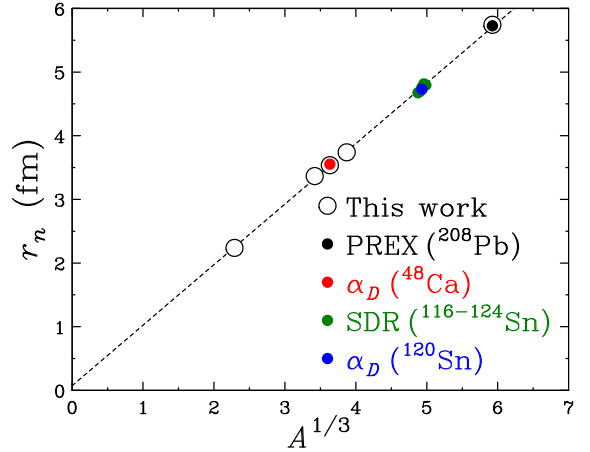


FIG. 12. Neutron radii  $r_n$  as a function of mass number  $A^{1/3}$ . The symbol “ $\alpha_D$ ” means the results of the  $E1$  polarizability experiment ( $E1pE$ ) for  $^{120}\text{Sn}$  [83] and  $^{48}\text{Ca}$  [44]. The symbol “PREX” stands for the result deduced from  $r_{\text{skin}}^{208}$  (PREX2) =  $0.283 \pm 0.071$  fm. The symbol “SDR” shows the results [82] of the measurement based on the isovector spin-dipole resonances (SDR) in the Sb isotopes. Open circles stand for the results of this paper. The dashed line is a guide for the eyes. The data (closed circles with error bar) are taken from Refs. [5,44,82,83].

$^{40,48}\text{Ca}$ ,  $^{58}\text{Ni}$ , and  $^{208}\text{Pb}$ , our results are added. Our results are consistent with the previous works.

#### ACKNOWLEDGMENT

We would like to thank Dr. Toyokawa for providing his code and Prof. M. Nakano for useful information.

- [1] X. Roca-Maza, M. Centelles, X. Vinas, and M. Warda, *Phys. Rev. Lett.* **106**, 252501 (2011).
- [2] C. J. Horowitz, S. J. Pollock, P. A. Souder, and R. Michaels, *Phys. Rev. C* **63**, 025501 (2001).
- [3] S. Abrahamyan, Z. Ahmed, H. Albatineh, K. Aniol, D. S. Armstrong, W. Armstrong, T. Averett, B. Babineau, A. Barbieri, V. Bellini *et al.* (PREX Collaboration), *Phys. Rev. Lett.* **108**, 112502 (2012).
- [4] C. J. Horowitz, Z. Ahmed, C.-M. Jen, A. Rakhman, P. A. Souder, M. M. Dalton, N. Livanage, K. D. Paschke, K. Saenboonruang, R. Silwal, G. B. Franklin, M. Friend, B. Quinn, K. S. Kumar, D. McNulty, L. Mercado, S. Riordan, J. Wexler, R. W. Michaels, and G. M. Urciuoli, *Phys. Rev. C* **85**, 032501(R) (2012).
- [5] D. Adhikari *et al.* (PREX), *Phys. Rev. Lett.* **126**, 172502 (2021).
- [6] A. Trzcińska, J. Jastrzbski, P. Lubiński, F. J. Hartmann, R. Schmidt, T. von Egidy, and B. Kłos, *Phys. Rev. Lett.* **87**, 082501 (2001).
- [7] J. Zenihiro, H. Sakaguchi, T. Murakami, M. Yosoi, Y. Yasuda, S. Terashima, Y. Iwao *et al.*, *Phys. Rev. C* **82**, 044611 (2010).
- [8] A. Tamii, I. Poltoratska, P. von Neumann-Cosel, Y. Fujita, T. Adachi, C. A. Bertulani, J. Carter *et al.*, *Phys. Rev. Lett.* **107**, 062502 (2011).
- [9] C. M. Tarbert, D. P. Watts, D. I. Glazier, P. Aguar, J. Ahrens, J. R. M. Annand, H. J. Arends, R. Beck, V. Bekrenev, B. Boillat *et al.* (Crystal Ball at MAMI and A2 Collaboration), *Phys. Rev. Lett.* **112**, 242502 (2014).
- [10] M. C. Atkinson, M. H. Mahzoon, M. A. Keim, B. A. Bordelon, C. D. Pruitt, R. J. Charity, and W. H. Dickhoff, *Phys. Rev. C* **101**, 044303 (2020).
- [11] D. Adhikari *et al.* (CREX), *Phys. Rev. Lett.* **129**, 042501 (2022).
- [12] S. J. Novario, G. Hagen, G. R. Jansen, and T. Papenbrock, *Phys. Rev. C* **102**, 051303(R) (2020).
- [13] H. Shen, F. Ji, J. Hu, and K. Sumiyoshi, *Astrophys. J.* **891**, 148 (2020).
- [14] C. Horowitz, *Ann. Phys. (NY)* **411**, 167992 (2019).
- [15] J.-B. Wei, J.-J. Lu, G. F. Burgio, Z.-H. Li, and H.-J. Schulze, *Eur. Phys. J. A* **56**, 63 (2020).
- [16] M. Thiel, C. Sienti, J. Piekarewicz, C. J. Horowitz, and M. Vanderhaeghen, *J. Phys. G: Nucl. Part. Phys.* **46**, 093003 (2019).
- [17] B. T. Reed, F. J. Fattoyev, C. J. Horowitz, and J. Piekarewicz, *Phys. Rev. Lett.* **126**, 172503 (2021).
- [18] S. Tagami, T. Wakasa, M. Takechi, J. Matsui, and M. Yahiro, *Results Phys.* **33**, 105155 (2022).



- [19] A. Akmal, V. R. Pandharipande, and D. G. Ravenhall, *Phys. Rev. C* **58**, 1804 (1998).
- [20] C. Ishizuka, T. Suda, H. Suzuki, A. Ohnishi, K. Sumiyoshi, and H. Toki, *Publ. Astron. Soc. Jpn.* **67**, 13 (2015).
- [21] C. Gonzalez-Boquera, M. Centelles, X. Viñas, and L. M. Robledo, *Phys. Lett. B* **779**, 195 (2018).
- [22] M. Farine, D. Von-Eiff, P. Schuck, J. F. Berger, J. Dechargé, and M. Girod, *J. Phys. G: Nucl. Part. Phys.* **25**, 863 (1999).
- [23] C. Gonzalez-Boquera, M. Centelles, X. Viñas, and A. Rios, *Phys. Rev. C* **96**, 065806 (2017).
- [24] M. Oertel, M. Hempel, T. Klähn, and S. Typel, *Rev. Mod. Phys.* **89**, 015007 (2017).
- [25] J. Piekarewicz, *Phys. Rev. C* **76**, 064310 (2007).
- [26] Y. Lim, K. Kwak, C. H. Hyun, and C.-H. Lee, *Phys. Rev. C* **89**, 055804 (2014).
- [27] R. Sellahewa and A. Rios, *Phys. Rev. C* **90**, 054327 (2014).
- [28] T. Inakura and H. Nakada, *Phys. Rev. C* **92**, 064302 (2015).
- [29] F. J. Fattoyev and J. Piekarewicz, *Phys. Rev. Lett.* **111**, 162501 (2013).
- [30] A. W. Steiner, M. Prakash, J. M. Lattimer, and P. J. Ellis, *Phys. Rep.* **411**, 325 (2005).
- [31] M. Centelles, X. Roca-Maza, X. Vinas, and M. Warda, *Phys. Rev. C* **82**, 054314 (2010).
- [32] M. Dutra, O. Lourenco, J. S. Sa Martins, A. Delfino, J. R. Stone, and P. D. Stevenson, *Phys. Rev. C* **85**, 035201 (2012).
- [33] B. A. Brown and A. Schwenk, *Phys. Rev. C* **89**, 011307(R) (2014); **91**, 049902 (2015).
- [34] B. A. Brown, *Phys. Rev. Lett.* **85**, 5296 (2000).
- [35] P. G. Reinhard, A. S. Umar, P. D. Stevenson, J. Piekarewicz, V. E. Oberacker, and J. A. Maruhn, *Phys. Rev. C* **93**, 044618 (2016).
- [36] C. Y. Tsang, B. A. Brown, F. J. Fattoyev, W. G. Lynch, and M. B. Tsang, *Phys. Rev. C* **100**, 062801(R) (2019).
- [37] C. Ducoin, J. Margueron, and C. Providencia, *Europhys. Lett.* **91**, 32001 (2010).
- [38] M. Fortin, C. Providencia, A. R. Raduta, F. Gulminelli, J. L. Zdunik, P. Haensel, and M. Bejger, *Phys. Rev. C* **94**, 035804 (2016).
- [39] L.-W. Chen, C. M. Ko, B.-A. Li, and J. Xu, *Phys. Rev. C* **82**, 024321 (2010).
- [40] P. W. Zhao and S. Gandolfi, *Phys. Rev. C* **94**, 041302(R) (2016).
- [41] Z. Zhang, Y. Lim, J. W. Holt, and C. M. Ko, *Phys. Lett. B* **777**, 73 (2018).
- [42] Y. Wang, C. Guo, Q. Li, H. Zhang, Y. Leifels, and W. Trautmann, *Phys. Rev. C* **89**, 044603 (2014).
- [43] O. Lourenço, M. Bhuyan, C. H. Lenzi, M. Dutra, C. Gonzalez-Boquera, M. Centelles, and X. Viñas, *Phys. Lett. B* **803**, 135306 (2020).
- [44] J. Birkhan *et al.*, *Phys. Rev. Lett.* **118**, 252501 (2017).
- [45] S. Tagami, T. Wakasa, J. Matsui, M. Yahiro, and M. Takechi, *Phys. Rev. C* **104**, 024606 (2021).
- [46] M. Matsuzaki, S. Tagami, and M. Yahiro, *Phys. Rev. C* **104**, 054613 (2021).
- [47] M. Toyokawa, M. Yahiro, T. Matsumoto, and M. Kohno, *Prog. Theor. Exp. Phys.* **2018**, 023D03 (2018).
- [48] S. Tagami, M. Tanaka, M. Takechi, M. Fukuda, and M. Yahiro, *Phys. Rev. C* **101**, 014620 (2020).
- [49] R. F. Carlson, A. J. Cox, J. R. Nimmo, N. E. Davison, S. A. Elbakr, J. L. Horton, A. Houdayer, A. M. Sourkes, W. T. H. Van Oers, and D. J. Margaziotis, *Phys. Rev. C* **12**, 1167 (1975).
- [50] A. Ingemarsson *et al.*, *Nucl. Phys. A* **653**, 341 (1999).
- [51] A. Auce *et al.*, *Phys. Rev. C* **71**, 064606 (2005).
- [52] A. B. Jones and B. A. Brown, *Phys. Rev. C* **90**, 067304 (2014).
- [53] S. Kox, A. Gamp, C. Perrin, J. Arvieux, R. Bertholet, J. F. Bruandet, M. Buenerd, Y. El Masri, N. Longequeue, and F. Merchez, *Phys. Lett. B* **159**, 15 (1985).
- [54] F. Brieva and J. Rook, *Nucl. Phys. A* **291**, 299 (1977); **291**, 317 (1977); **297**, 206 (1978).
- [55] G. Satchler and W. Love, *Phys. Rep.* **55**, 183 (1979); G. R. Satchler, *Direct Nuclear Reactions* (Oxford University Press, New York, 1983).
- [56] N. Yamaguchi, S. Nagata, and T. Matsuda, *Prog. Theor. Phys.* **70**, 459 (1983); S. Nagata, M. Kamimura, and N. Yamaguchi, *ibid.* **73**, 512 (1985); N. Yamaguchi, S. Nagata, and J. Michiyama, *ibid.* **76**, 1289 (1986).
- [57] K. Amos, P. J. Dortmans, H. V. von Geramb, S. Karataglidis, and J. Raynna, in *Advances in Nuclear Physics*, edited by J. W. Negele and E. Vogt (Springer, New York, 2000), pp. 276–536.
- [58] T. Furumoto, Y. Sakuragi, and Y. Yamamoto, *Phys. Rev. C* **78**, 044610 (2008); **79**, 011601(R) (2009); **80**, 044614 (2009).
- [59] K. Egashira, K. Minomo, M. Toyokawa, T. Matsumoto, and M. Yahiro, *Phys. Rev. C* **89**, 064611 (2014).
- [60] M. Toyokawa, K. Minomo, M. Kohno, and M. Yahiro, *J. Phys. G: Nucl. Part. Phys.* **42**, 025104 (2015); **44**, 079502 (2017).
- [61] M. Toyokawa, M. Yahiro, T. Matsumoto, K. Minomo, K. Ogata, and M. Kohno, *Phys. Rev. C* **92**, 024618 (2015); **96**, 059905(E) (2017).
- [62] K. Minomo, T. Sumi, M. Kimura, K. Ogata, Y. R. Shimizu, and M. Yahiro, *Phys. Rev. Lett.* **108**, 052503 (2012).
- [63] M. Takechi *et al.*, *Phys. Lett. B* **707**, 357 (2012).
- [64] T. Sumi, K. Minomo, S. Tagami, M. Kimura, T. Matsumoto, K. Ogata, Y. R. Shimizu, and M. Yahiro, *Phys. Rev. C* **85**, 064613 (2012).
- [65] S. Watanabe, K. Minomo, M. Shimada, S. Tagami, M. Kimura, M. Takechi, M. Fukuda, D. Nishimura, T. Suzuki, T. Matsumoto *et al.*, *Phys. Rev. C* **89**, 044610 (2014).
- [66] T. Eliyakut-Roshko, R. H. McCamis, W. T. H. van Oers, R. F. Carlson, and A. J. Cox, *Phys. Rev. C* **51**, 1295 (1995).
- [67] J. F. Dicello, G. J. Igo, and M. L. Roush, *Phys. Rev.* **157**, 1001 (1967).
- [68] P. J. Bulman and J. A. R. Griffith, *Nucl. Phys. A* **111**, 315 (1968).
- [69] R. F. Carlson, A. J. Cox, N. E. Davison, T. Eliyakut-Roshko, R. H. McCamis, and W. T. H. van Oers, *Phys. Rev. C* **49**, 3090 (1994).
- [70] J. J. H. Menet, E. E. Gross, J. J. Malanify, and A. Zucker, *Phys. Rev. C* **4**, 1114 (1971).
- [71] T. Wakasa, S. Tagami, J. Matsui, M. Yahiro, and M. Takechi, *Results Phys.* **29**, 104749 (2021).
- [72] J. Fujita and H. Miyazawa, *Prog. Theor. Phys.* **17**, 360 (1957); **17**, 366 (1957).
- [73] M. Kohno, *Phys. Rev. C* **88**, 064005 (2013); **96**, 059903(E) (2017).
- [74] H. V. von Geramb, K. Amos, L. Berge, S. Bräutigam, H. Kohlhoff, and A. Ingemarsson, *Phys. Rev. C* **44**, 73 (1991).
- [75] P. J. Dortmans and K. Amos, *Phys. Rev. C* **49**, 1309 (1994).
- [76] K. Minomo, K. Ogata, M. Kohno, Y. R. Shimizu, and M. Yahiro, *J. Phys. G: Nucl. Part. Phys.* **37**, 085011 (2010).
- [77] I. Angeli and K. P. Marinova, *At. Data Nucl. Data Tables* **99**, 69 (2013).
- [78] J. Zenihiro *et al.*, [arXiv:1810.11796](https://arxiv.org/abs/1810.11796).

- [79] I. Tanihata, T. Kobayashi, O. Yamakawa, S. Shimoura, K. Ekuni, K. Sugimoto, N. Takahashi, T. Shimoda, and H. Sato, *Phys. Lett. B* **206**, 592 (1988).
- [80] J. C. Zamora *et al.*, *Phys. Rev. C* **96**, 034617 (2017).
- [81] A. Ozawa, T. Suzuki, and I. Tanihata, *Nucl. Phys. A* **693**, 32 (2001).
- [82] A. Krasznahorkay *et al.*, *Phys. Rev. Lett.* **82**, 3216 (1999).
- [83] T. Hashimoto, A. M. Krumbholz, P. G. Reinhard, A. Tamii, P. von Neumann-Cosel, T. Adachi, N. Aoi, C. A. Bertulani, H. Fujita, Y. Fujita, E. Ganioglu, K. Hatanaka, E. Ideguchi, C. Iwamoto, T. Kawabata, N. T. Khai, A. Krugmann, D. Martin, H. Matsubara, K. Miki *et al.*, *Phys. Rev. C* **92**, 031305(R) (2015).